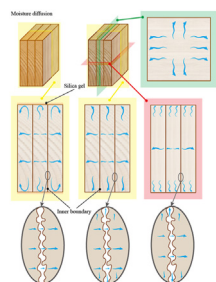Research article

# An inner boundary condition of moisture diffusion model for simulating transient nonlinear moisture transport in Chinese fir

Xueyi Ma, Dong Zhao, Chenyu Yao, Jian Zhao [*]

*School of Technology, Beijing Forestry University, Beijing, 100083, China*

## GRAPHICAL ABSTRACT

ABSTRACT

This paper proposed an inner boundary condition of moisture diffusion model for simulating transient nonlinear moisture transport of Chinese fir (*Cunninghamia lanceolata*). The inner boundary condition is serviced for simulate the moisture diffusion of multi-layer boards and is mainly used for the boundary conditions inside component, which presents the diffusion of moisture between wood and its adjacent wood. Furthermore, the established simulation model contains fiber orientation information and is used to simulate the moisture diffusion under different boundary conditions, which considers the constrained boundary. Simulation of simple boundary condition models and the proposed inner boundary condition model under different boundary conditions for multilayer board specimen exposed to constant temperature and constant humidity with a known initial moisture content, and the model was then validated in a laboratory climate chamber. Different from the simple boundary condition model the direct error of the proposed inner boundary model was less than 2% (moisture content), which indicates the proposed inner boundary condition could improve the accuracy of moisture diffusion model. The results show that the inner boundary condition model can comprehensively analyze the transient nonlinear moisture transfer process in different fiber directions with high accuracy.

## 1. Introduction

With the increasing awareness of low carbon [1], wood is considered as a vital material of sustainable development strategy, because of its renewable and low-carbon [2]. It is well known that wood plays an important role in the field of biomass fuel [3], and it has also been applied in the field of civil engineering (construction). Due to its light weight, easy construction, and environmentally friendly, the wood-frame constructions are regarded as one of the main building types in the world. And wood is used to construct different forms of constructions, such as

the residential buildings in North America [4], Han-Ok in Korea [5], ships in ancient China [6], various bridges [7], etc. However, the performance of wood-frame is affected by many factors during construction and in service. The wood-frame will experience moisture absorption and desorption spontaneously with long-term exposure to an unstable humidity environment. The moisture absorption and desorption phenomenon of wood not only affects its mechanical properties [8], such as structural failure caused by cracks [9] and deformation [10], but also causes pathological phenomena such as fungal erosion [7], which leads to the decay of wood. The monitoring of the moisture content of wood-frame can be used not only to judge the mold grade [11], but also to evaluate the material degradation and predict the service life [12, 13]. Hence, the monitoring and prediction of the moisture content of wood-frames is very important.

With the development of numerical simulation technology, the method for studying hygrothermal model of wood-frame construction have also been developed [14, 15]. And the hygrothermal model has been widely used in the field of moisture absorption and desorption of wood. For example, one-dimensional moisture diffusion phenomenon of wood can be described by the one-dimensional evaporation interface mathematical model [16]. Although the moisture diffusion of wood can quantitatively analyze the moisture transfer law at the end of the wood beam [17], the one-dimensional moisture diffusion model is different from the actual diffusion process, which led to the development of a two-dimensional and three-dimensional diffusion model for studying the ends of wood beams [18]. Since humidity not only affects the durability of a single wood-frame but also affects the overall performance of the building [19, 20], the more complex the wood-frame-construction, the more difficult it is to establish a moisture diffusion model. Whether it is a wood frame beam [18] or a wood fiber thermal insulation frame [21], the study of humidity is research of simple shapes and specific environments. In the study of the balance equation of moisture diffusion model based on Fick's second law [22, 23, 24, 25, 26], the use of nonlinear single-Fickian models combined with nonlinear Neumann boundary conditions can describe not only slow MC changes [27, 28] but also fast MC changes [29], but both of which are only direct the single wooden specimen. The actual wood frame construction is not the moisture absorption or desorption of a single wood frame in a stable state, but the moisture absorption and desorption of multiple wood frame specimens under different conditions. Hence, the impacts of moisture diffusion on balance equation at wood-frame construction is one of the most difficult challenges.

For the purpose of solve the above problems, the aim of this paper is to provides a inner boundary condition serviced for wood-frame construction moisture diffusion controlled by the boundary conditions, which is used for the moisture analysis of wood-frame construction in complex situations. Serving the above aim, a multi-boundary condition adaptive diffusion equation for multi-layer boards based on Fick's second law is established. By entering the corresponding parameters and selecting the specified boundary conditions, the moisture content distribution of the multi-layer board can be predicted. Section 2 details the moisture diffusion model with inner boundary condition for numerical solution of three-layer board with difference boundary conditions. Section 3 presents actual experiment and simulation experiment, and a simple boundary model was used for complementary comparisons. Section 4 shows the result and the effectiveness of the proposed inner boundary condition, which is verified by comparing the actual experiment and simple boundary model with the proposed inner boundary simulation. Section 5 is the conclusion and the shortcomings of this method.

## 2. Principle

The transient moisture diffusion process in the solid drying process is close to the heat conduction process of the solid. The form of the governing equation is the same as the Fourier equation for heat transfer, in which concentration is used instead of temperature, and moisture diffusion coefficient is used instead of thermal diffusivity [30].

Assuming that the thermophysical properties of wood and drying medium are fixed values, and the influence of heat transfer on moisture diffusion is negligible under constant temperature conditions [31]. Suppose the size of each board is $2L_x \times 2L_y \times 2L_z$, and the internal moisture content of each board is uniform in the initial state. And the moisture diffusion coefficient and the mass diffusivity coefficient of every layer board are not influenced by the space of the wood board.

### 2.1. Moisture diffusion model of board

#### 2.1.1. The governing equation of moisture diffusion

In one-dimensional diffusion, assuming that moisture diffusion occurs in only one direction of the board, the governing equation for transient moisture diffusion is as shown in Eq. (1).

$$\frac{\partial M}{\partial t} = D \frac{\partial^2 M}{\partial x^2} \tag{1}$$

where, $M$ represents the wood moisture content, $t$ represents the diffusion time, D represents the moisture diffusion coefficient, and $x$ represents the coordinate position along the diffusion direction. It should be noted that the origin of the coordinates is in the center of the board.

In the two-dimensional moisture diffusion model, assuming that moisture diffusion occurs in two different directions of the board, the governing equation of transient moisture diffusion is as shown in Eq. (2).

$$\frac{\partial M}{\partial t}(x,y,t) = D_1 \frac{\partial^2 M}{\partial x^2}(x,y,t) + D_2 \frac{\partial^2 M}{\partial y^2}(x,y,t) \tag{2}$$

where, $x$ and $y$ represent the coordinate position along the respective diffusion direction.

In the three-dimensional moisture diffusion model, assuming that moisture diffusion occurs in all direction of the board, the governing equation of transient moisture diffusion is as shown in Eq. (3).

$$\frac{\partial M}{\partial t}(x,y,z,t) = D_1 \frac{\partial^2 M}{\partial x^2}(x,y,z,t) + D_2 \frac{\partial^2 M}{\partial y^2}(x,y,z,t) + D_3 \frac{\partial^2 M}{\partial z^2}(x,y,z,t) \tag{3}$$

where, $x$, $y$ and $z$ represent the coordinate position along the respective diffusion direction.

#### 2.1.2. The initial and boundary conditions

The initial condition is as shown in Eq. (4).

$$M|_{t=0} = M_i \tag{4}$$

There are three boundary conditions in the actual moisture diffusion process: insulating surface; surface in contact with air; surface in contact with other substances.

The mass transfer at this location is constant with 0 during this process, which is a Neumann boundary condition. Assuming that the moisture of the board diffuses outward along the neutral layer, the boundary condition at the neutral layer of the board is the Neumann boundary condition [32] as shown in Eq. (5).

$$\frac{\partial M}{\partial [*]}\Big|_{[*]=X} = 0 \tag{5}$$

where, $[*]$ indicates the diffusion direction; $X$ indicates the coordinate of surface, which is insulating surface.

The latter two types of boundary types can be classified into one type. When the surface exchanges moisture with the other objects, the relationship between the two can be inferred from Newton's test law in heat conduction problem, knows as the third type of boundary conditions [33] as shown in Eq. (6).

$$-D_i\left(\frac{\partial M}{\partial[*]}\Big|_{[*]=X}\right) = k_i M|_{[*]=X} \tag{6}$$

where, $X$ indicates the coordinate of surface, which is surface in contact with other object; $D_i$ indicates the moisture diffusion coefficient in $[*]$ direction; and $k_i$ represent the surface emission coefficient of the boundary.

### 2.2. Moisture diffusion mathematical model of different condition

#### 2.2.1. Three-layer board with constrained boundary

When there is no diffusion around the three-layer board (Figure 2(c)), which is called the constrained boundary. The moisture diffuses outward along the neutral layer, thus the mathematical model with constrained boundary was established as 1/8 of the neutral layer outwards as shown in Eq. (7) and the coordinate system is as shown in Figure 7(b).

$$\begin{cases} \dfrac{\partial M_1}{\partial t}(z,t) = D_{1,z}\dfrac{\partial^2 M_1}{\partial z^2}(z,t) & (x \in [0, L_x], y \in [0, L_y], z \in [0, L_z]) \\ \dfrac{\partial M_2}{\partial t}(z,t) = D_{2,z}\dfrac{\partial^2 M_2}{\partial z^2}(z,t) & (x \in [0, L_x], y \in [0, L_y], z \in [L_z, 3L_z]) \end{cases} \tag{7}$$

where, the first number of the subscript indicates the middle or outer board (1 indicates the middle board; and 2 indicates the outer board); the letter of the subscript indicates the diffusion direction.

Assuming that the initial moisture content in each layer of wood is uniform. The initial condition can be expressed as follows:

$$\begin{cases} M_1|_{t=0} = M_{i1} \\ M_2|_{t=0} = M_{i2} \end{cases} \tag{8}$$

where, $M_{i1}$ indicates the initial moisture content of middle board and $M_{i2}$ indicates the initial moisture content of outer board; the number of the subscript indicates the middle or outer board (1 indicates the middle board; and 2 indicates the outer board).

Since the sides of the three-layer board were sealed, the moisture diffusion is only in the thickness direction (z-direction). The boundary condition is as follows:

$$\begin{cases} \dfrac{\partial M}{\partial x}\Big|_{x=0} = 0 \\ \dfrac{\partial M}{\partial y}\Big|_{y=0} = 0 \\ \dfrac{\partial M}{\partial z}\Big|_{z=0} = 0 \\ \dfrac{\partial M}{\partial x}\Big|_{x=L_x} = 0 \\ \dfrac{\partial M}{\partial y}\Big|_{y=L_y} = 0 \\ -D_{1,z}\left(\dfrac{\partial M_1}{\partial z}\Big|_{z=L_z}\right) = k_{1,z}M_1|_{z=L_z} \\ -D_{2,z}\left(\dfrac{\partial M_2}{\partial z}\Big|_{z=3L_z}\right) = k_{2,z}M_2|_{z=3L_z} \end{cases} \tag{9}$$

where, the number of the subscript indicates the middle or outer board (1 indicates the middle board; and 2 indicates the outer board); $k_{1,z}$ represents the surface emission coefficient between the middle and external board and $k_{2,z}$ represents the surface emission coefficient between the external board and air. And the 6th equation in Eq. (9) indicates the boundary condition inside the wood frame under constrained boundary condition. The 6th equation in Eq. (9) presents the inner boundary condition.

The numerical solution by using the finite difference method is Eq. (10), and **Supplementary Material (Appendix A)** details the solution process.

$$\begin{cases} \vec{M}_1^{n+1} = \vec{M}_1^n + D_{1,z}\dfrac{1}{\Delta Z^2}\vec{M}_{1,xz}^n A\Delta t \\ \vec{M}_2^{n+1} = \vec{M}_2^n + D_{2,z}\dfrac{1}{\Delta Z^2}\vec{M}_{2,xz}^n A\Delta t \\ \vec{M}_{yz}^{n+1}\big|_{x=0} = \vec{M}_{yz}^n\big|_{x=0} \\ \vec{M}_{yz}^{n+1}\big|_{x=L_x} = \vec{M}_{yz}^n\big|_{x=L_x} \\ \vec{M}_{xz}^{n+1}\big|_{y=0} = \vec{M}_{xz}^n\big|_{y=0} \\ \vec{M}_{xz}^{n+1}\big|_{y=L_y} = \vec{M}_{xz}^n\big|_{y=L_y} \\ \vec{M}_{xy}^{n+1}\big|_{z=0} = \vec{M}_{xy}^n\big|_{z=0} \\ \vec{M}_{1,xy}^n\big|_{z=(N_z+1)} = \dfrac{D_{1,z}}{D_{1,z}+k_{1,z}\Delta z}\vec{M}_{1,xy}^n\big|_{z=(N_z+1)}(N_z = L_z/\Delta z) \\ \vec{M}_{2,xy}^n\big|_{z=3(N_z+1)} = \dfrac{D_{2,z}}{D_{2,z}+k_{2,z}\Delta z}\vec{M}_{2,xy}^n\big|_{z=3(N_z+1)}(N_z = L_z/\Delta z) \\ \vec{M}^0 = M^0 \ (x=0 \text{ or } y=0 \text{ or } z=0 \text{ or } x=L_x \text{ or } y=L_y) \end{cases} \tag{10}$$

where, $\vec{M}$ represents the matrix form of $M$; the $xy$, $xz$ and $yz$ of the subscript indicates the moisture content matrix in the $xy$-plane, $xz$-plane and $yz$-plane. And A is as shown in Eq. (11).

$$A = \begin{bmatrix} -2 & 1 & 0 & 0 & \cdots & 0 & 0 \\ 1 & -2 & 1 & 0 & \cdots & 0 & 0 \\ 0 & 1 & -2 & 1 & \cdots & 0 & 0 \\ \vdots & \vdots & \vdots & \vdots & \ddots & \vdots & \vdots \\ 1 & 0 & 0 & 0 & 0 & 1 & -2 \end{bmatrix} \tag{11}$$

#### 2.2.2. Three-layer board with free boundary

When the diffusion in all directions of the three-layer board is unconstrained, which is called free boundary. The governing equation of moisture diffusion in three-layer board with free boundary is as shown in Eq. (12).

$$\begin{cases} \dfrac{\partial M_1}{\partial t}(x,y,z,t) = D_{1,x}\dfrac{\partial^2 M_1}{\partial x^2}(x,y,z,t) + D_{1,x}\dfrac{\partial^2 M_1}{\partial y^2}(x,y,z,t) + D_{1,z}\dfrac{\partial^2 M_1}{\partial z^2}(x,y,z,t) \\ \qquad (x \in [0, L_x], y \in [0, L_y], z \in [0, L_z]) \\ \dfrac{\partial M_2}{\partial t}(x,y,z,t) = D_{2,x}\dfrac{\partial^2 M_2}{\partial x^2}(x,y,z,t) + D_{2,x}\dfrac{\partial^2 M_2}{\partial y^2}(x,y,z,t) + D_{2,z}\dfrac{\partial^2 M_2}{\partial z^2}(x,y,z,t) \\ \qquad (x \in [0, L_x], y \in [0, L_y], z \in [L_z, 3L_z]) \end{cases} \tag{12}$$

And the initial condition is also same as Eq. (8). Since the sides of the three-layer board were free, the moisture diffusion is in all directions (x-direction, y-direction and z-direction). The boundary condition is as follows:

$$\begin{cases} \dfrac{\partial M}{\partial x}\Big|_{x=0} = 0 \\ \dfrac{\partial M}{\partial y}\Big|_{y=0} = 0 \\ \dfrac{\partial M}{\partial z}\Big|_{z=0} = 0 \\ -D_{1,x}\left(\dfrac{\partial M_1}{\partial x}\Big|_{x=L_x}\right) = k_{1,x}M_1|_{x=L_x} \\ -D_{2,x}\left(\dfrac{\partial M_2}{\partial x}\Big|_{x=L_x}\right) = k_{2,x}M_2|_{x=L_x} \\ -D_{1,y}\left(\dfrac{\partial M_1}{\partial y}\Big|_{y=L_y}\right) = k_{1,y}M_1|_{y=L_y} \\ -D_{2,y}\left(\dfrac{\partial M_2}{\partial y}\Big|_{y=L_y}\right) = k_{2,y}M_2|_{y=L_y} \\ -D_{1,z}\left(\dfrac{\partial M_1}{\partial z}\Big|_{z=L_z}\right) = k_{1,z}M_1|_{z=L_z} \\ -D_{2,z}\left(\dfrac{\partial M_2}{\partial z}\Big|_{z=3L_z}\right) = k_{2,z}M_2|_{z=3L_z} \end{cases} \tag{13}$$

And the 8th equation in Eq. (13) indicates the boundary condition inside the wood frame under free boundary condition, which was called the inner boundary conditions.

The numerical solution obtained by using the finite difference method is Eq. (14), and **Supplementary Material (Appendix A)** details the solution process.

$$
\begin{cases}
\vec{M}_1^{n+1} = \vec{M}_1^n + (D_{1,x}\frac{1}{\Delta x^2}A\vec{M}_{1,xy}^n + D_{1,y}\frac{1}{\Delta y^2}\vec{M}_{1,xy}^n A + D_{1,z}\frac{1}{\Delta z^2}\vec{M}_{1,xz}^n A)\Delta t \\
\vec{M}_2^{n+1} = \vec{M}_2^n + (D_{2,x}\frac{1}{\Delta x^2}A\vec{M}_{2,xy}^n + D_{2,y}\frac{1}{\Delta y^2}\vec{M}_{2,xy}^n A + D_{2,z}\frac{1}{\Delta z^2}\vec{M}_{2,xz}^n A)\Delta t \\
\vec{M}_{yz}^{n+1}\big|_{x=0} = \vec{M}_{yz}^n\big|_{x=0} \\
\vec{M}_{xz}^{n+1}\big|_{y=0} = \vec{M}_{xz}^n\big|_{y=0} \\
\vec{M}_{xy}^{n+1}\big|_{z=0} = \vec{M}_{xy}^n\big|_{z=0} \\
\vec{M}_{1,yz}^{n+1}\big|_{x=N_x+1} = \frac{D_{1,x}}{D_{1,x}+k_{1,x}\Delta x}\vec{M}_{1,yz}^n\big|_{x=N_x} \ (N_x = L_x/\Delta x) \\
\vec{M}_{2,yz}^{n+1}\big|_{x=N_x+1} = \frac{D_{2,x}}{D_{2,x}+k_{2,x}\Delta x}\vec{M}_{2,yz}^n\big|_{x=N_x} \ (N_x = L_x/\Delta x) \\
\vec{M}_{1,xz}^{n+1}\big|_{y=N_y+1} = \frac{D_{1,y}}{D_{1,y}+k_{1,y}\Delta y}\vec{M}_{1,xz}^n\big|_{y=N_y} \ (N_y = L_y/\Delta y) \\
\vec{M}_{2,xz}^{n+1}\big|_{y=N_y+1} = \frac{D_{2,y}}{D_{2,y}+k_{2,y}\Delta y}\vec{M}_{2,xz}^n\big|_{y=N_y} \ (N_y = L_y/\Delta y) \\
\vec{M}_{1,xy}^n\big|_{z=N_z+1} = \frac{D_{1,z}}{D_{1,z}+k_{1,z}\Delta z}\vec{M}_{1,xy}^n\big|_{z=N_z+1} \ (N_z = L_z/\Delta z) \\
\vec{M}_{2,xy}^n\big|_{z=3(N_z+1)} = \frac{D_{2,z}}{D_{2,z}+k_{2,z}\Delta z}\vec{M}_{2,xy}^n\big|_{z=3(N_z+1)} \ (N_z = L_z/\Delta z) \\
\vec{M}^0 = M^0 \ (x = 0 \ or \ y = 0 \ or \ z = 0)
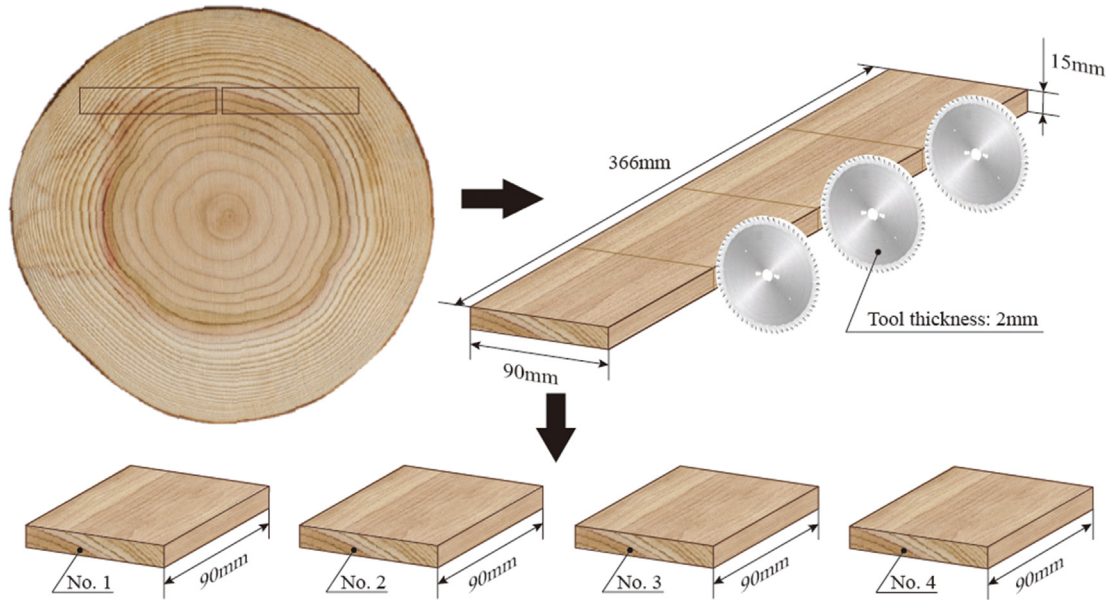\end{cases}
\tag{14}
$$



**Figure 1.** Schematic diagram of texture and position relationship.
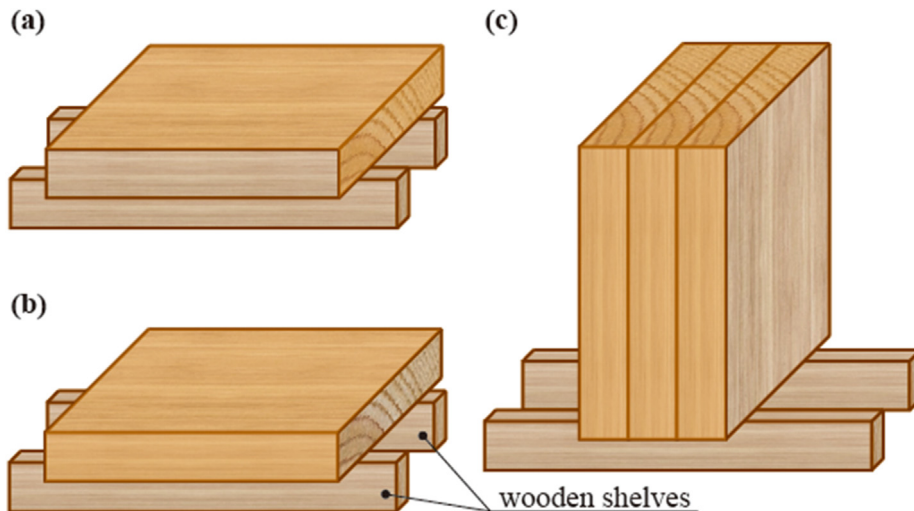


**Figure 2.** (a) Schematic diagram of the flux direction as T; (b) Schematic diagram of flux direction as L; (c) Schematic diagram of the flux direction as R with three-layer board.

## 3. Experiments

The material used in this manuscript was Chinese fir (*Cunninghamia lanceolata*) from Ningde, Fujian, China. Due to the excellent mechanical properties of quarter-sawed lumber, quarter-sawed lumber is widely used [34]. Therefore, the plate selected for the test is also a chord-cut plate. As shown in Figure 1 and 10 pieces of 366 mm × 90 mm × 15 mm boards were first cut out, which are free of defects. In order to reduce the influence of wood texture and properties between different groups as much as possible, the wood in similar positions was taken as the specimen: the left position and the right position in the log in Figure 1. The 10 wooden boards were divided into two groups, GI and GII, six groups with similar texture were selected as GI (marked as A-F groups), and four groups with similar texture were also selected as GII (marked as G-J groups). Each board was then cut into 4 equal parts in order (marked as No. 1, No. 2, No. 3, and No. 4). In order to reduce the influence of texture, some specimens were reused during the experiment.

### 3.1. Preparation before experiments

#### 3.1.1. Determine the coefficient of three-layer board

The moisture diffusion coefficient and surface emission coefficient of wood need to be determined before the formal experiment.

In this manuscript, Dincer's method [31, 35] was used to determine coefficients in all directions of the specimen. First, the 90 mm × 90 mm × 15 mm specimen was dried to a constant weight at (103 ± 2) °C to obtain the drying weight.

All the specimens were divided into 3 groups, the first group of 5 specimens, the surfaces texture of RT (radial-tangential) cut were the flux surface, and the other four surfaces were coated with silica gel (Figure 2(a)); the second group of 5 specimens, the longitudinal was the flux direction (Figure 2(b)), the remaining four surfaces were coated with silica gel; in the third group of 15 specimens, four sides (90 mm × 15 mm): the surfaces texture of RT (radial-tangential) cut, the surface texture of LR (longitudinal -radial) cut and the surfaces texture of LT (longitudinal -tangential) cut were coated with silica gel and fixed as shown in Figure 2(c). The specimens were then conditioned in a climate
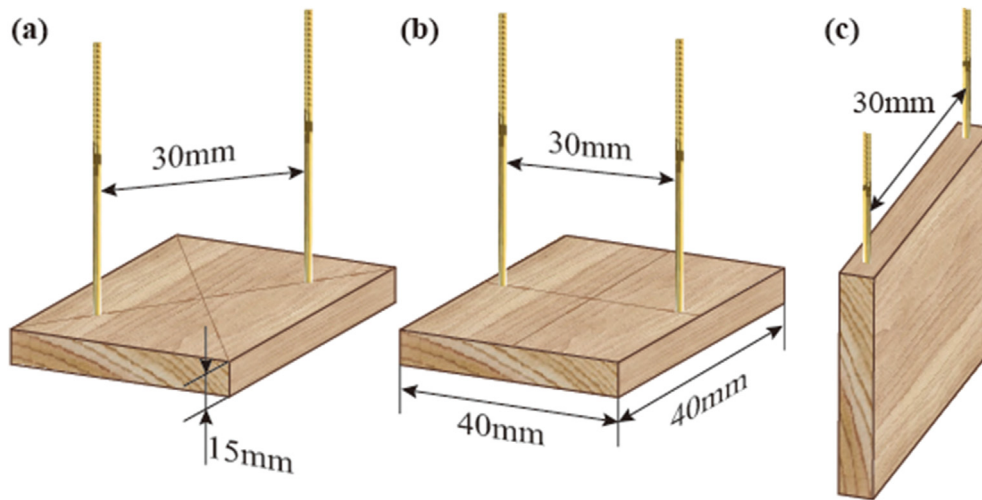


**Figure 3.** Schematic diagram of probe insertion for calibration. (a) The included angle with the longitudinal direction and measurement line is 45°; (b) The measurement line perpendicular to the longitudinal direction; (c) The measurement line parallel to the longitudinal direction.
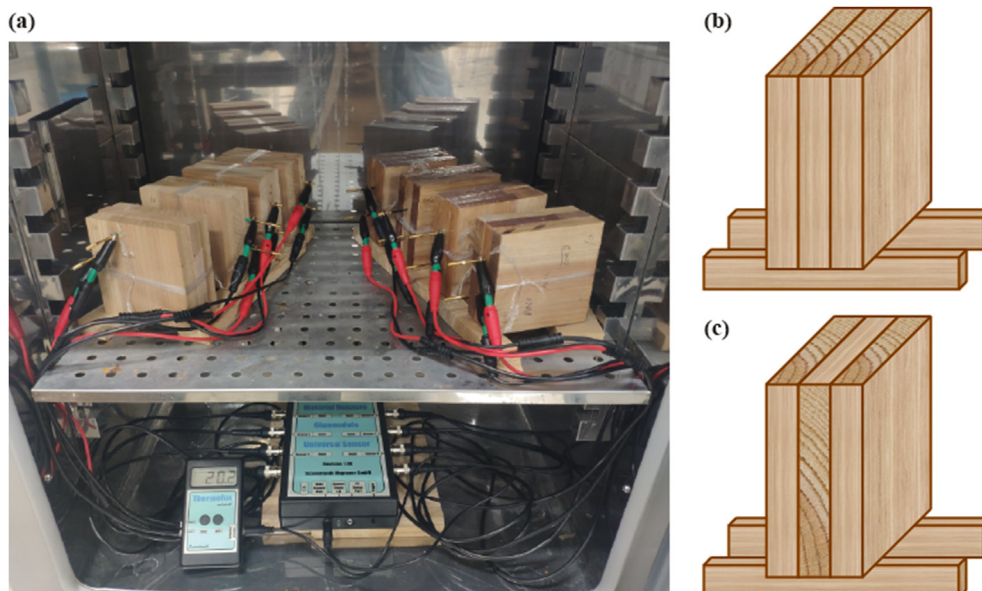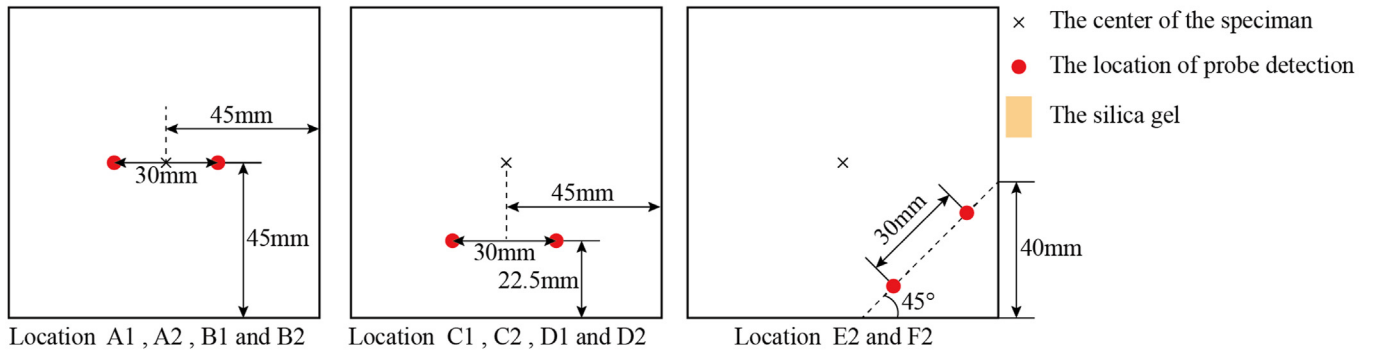


**Figure 4.** (a) Experiment configuration; (b) Schematic diagram of the test with parallel texture; (c) Schematic diagram of the test with vertical texture.

**(a) Schematic diagram of 2D measuring point location**



Location A1 , A2 , B1 and B2

Location C1 , C2 , D1 and D2

Location E2 and F2

- × The center of the speciman
- ● The location of probe detection
- ▮ The silica gel

**(b) Schematic diagram of 3D measuring point location**



Location A1

Location B1

Location C1

Location D1

Location A2

Location B2
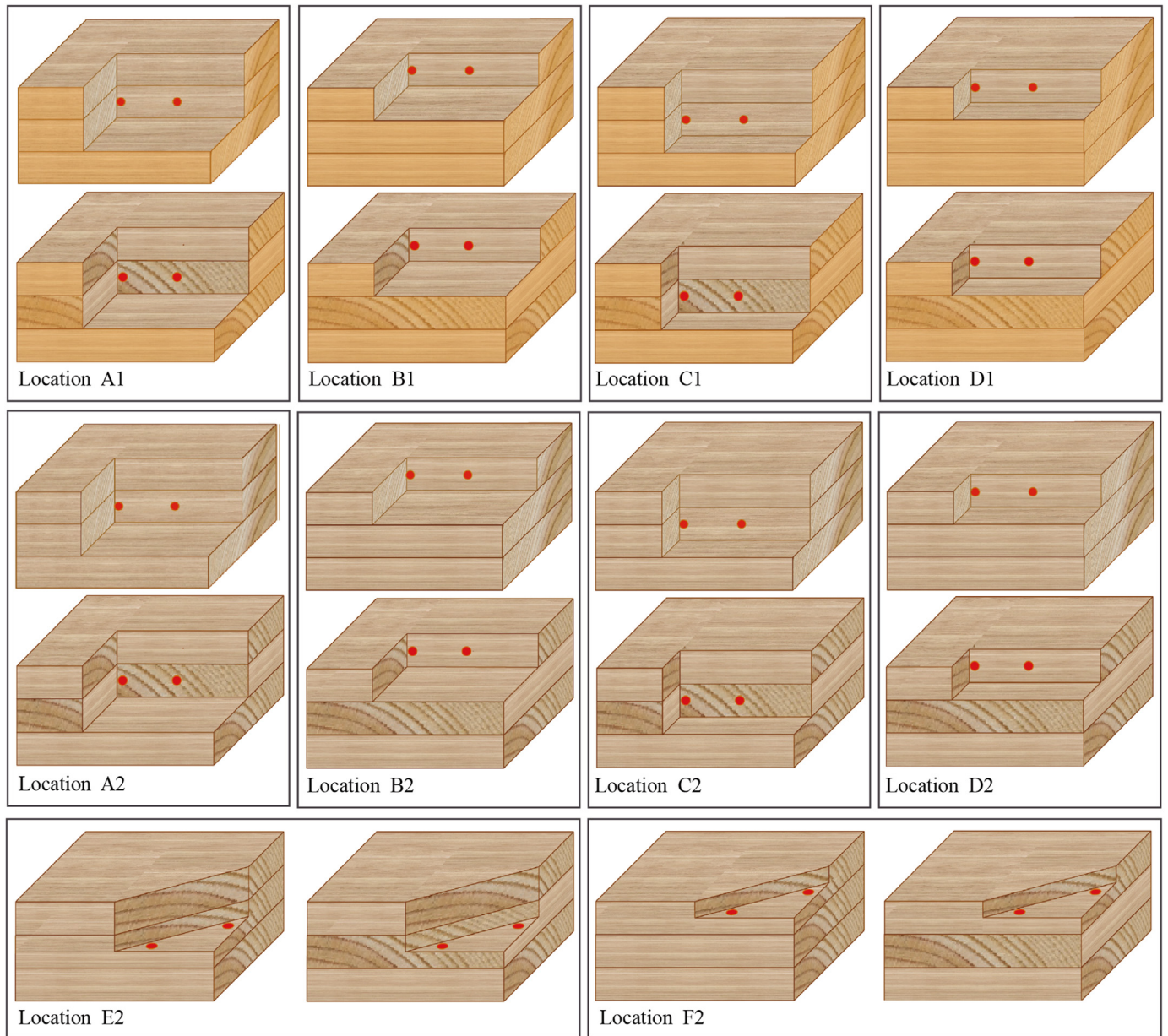
Location C2

Location D2

Location E2

Location F2

**Figure 5.** (a) Schematic diagram of distances of the measuring points to the edges; (b) Schematic diagram of measurement location.
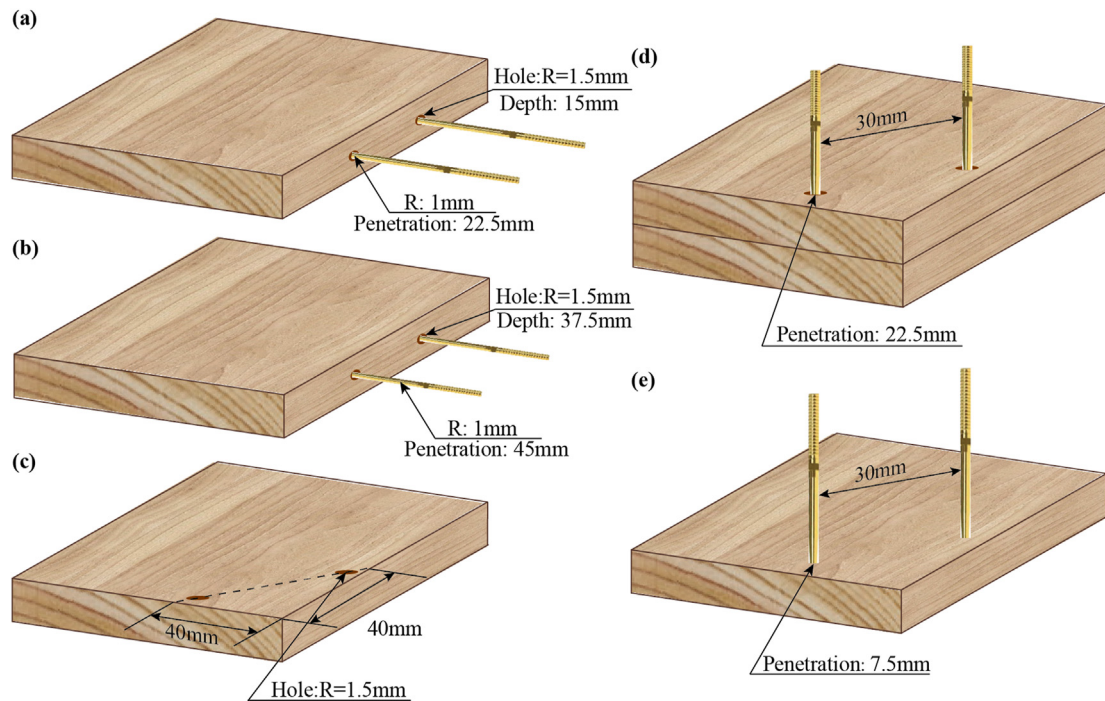
**Figure 6.** (a) Schematic diagram of probe insertion from the center of the board to the half of the boundary (b) Schematic diagram of probe insertion at center of the board; (c) Schematic diagram of distances of the measuring points near a corner; (d) Schematic diagram of probe insertion near a corner of the middle board; (e) Schematic diagram of probe insertion near a corner of the board.

**Table 1.** The initial moisture content of each layer board with parallel texture.

|  | The first layer board (%) | The middle layer board (%) | The third layer board (%) |
|---|---|---|---|
| Location A1 | 24.0 | 24.8 | 23.5 |
| Location B1 | 15.0 | 15.0 | 12.0 |
| Location C1 | 15.0 | 12.9 | 14.5 |
| Location D1 | 20.1 | 20.0 | 18.9 |
| Location A2 | 15.6 | 20.2 | 16 |
| Location B2 | 22.3 | 23.1 | 15.8 |
| Location C2 | 15.5 | 17.8 | 15.4 |
| Location D2 | 16.4 | 21.7 | 16.3 |
| Location E2 | 16.6 | 17.4 | 24.8 |
| Location F2 | 14.4 | 26.4 | 20.3 |

chamber with an air humidity of 90% and a temperature of 25 °C until the moisture in the specimen reached equilibrium, and the moisture content was below wood FSP. After the third group of specimens was

**Table 2.** The initial moisture content of each layer board with vertical texture.

|  | The first layer board (%) | The middle layer board (%) | The third layer board (%) |
|---|---|---|---|
| Location A1 | 12.0 | 12.8 | 12.3 |
| Location B1 | 20.1 | 20.0 | 15.8 |
| Location C1 | 20.0 | 15.0 | 15.4 |
| Location D1 | 17.8 | 18.0 | 15.5 |
| Location A2 | 19.0 | 19.0 | 18.5 |
| Location B2 | 21.4 | 21.4 | 20.3 |
| Location C2 | 15.0 | 20.2 | 15.9 |
| Location D2 | 18.0 | 21.0 | 17.8 |
| Location E2 | 12.0 | 19.4 | 15.5 |
| Location F2 | 14.8 | 24.2 | 15.6 |

fixed as shown in Figure 2(c), all specimens were placed in a climate chamber with an air humidity of 40% and a temperature of 25 °C, a precision balance (accuracy of 0.01 g) was used to measure the mass every 10 min for 48 h. Finally, the obtained desorption curves were processed according to Dincer's method to determine the moisture diffusion coefficient and surface emission coefficient in three directions.

Differ from the first and second group, the third group of middle-layer plates was treated as a single individual, and the first and third layers were treated as 90 mm × 90 mm × 30 mm specimens, which could determine the inner boundary inside the wood frame.

*3.1.2. Calibration of moisture content detector*

Since the wood species contained in the moisture content detector are different from those selected in this manuscript, the calibration of the moisture content detector is essential.

Take the No.4 specimen from groups A-E and G-J, and the specimens was cut into a smaller piece of 40 mm × 40 mm × 15 mm. Then the specimens were placed in a drying oven (Haowei WGL101-2A, Hebei, China) for absolute drying at a temperature of 103 ± 2 °C. And use a precision balance (accuracy of 0.01 g) to measure the mass every 2 h until the mass remains unchanged, which is the absolute dry weight of the specimen. Next, a group of 3 samples was inserted into the probe directly. Three types of probe-insertion were used for calibration of moisture content, Figure 3(a) shows the included angle with the longitudinal direction and measurement line is 45°, Figure 3(b) shows the measurement line perpendicular to the longitudinal direction and Figure 3(c) shows the measurement line parallel to the longitudinal direction. The specimens were then placed in a climate chamber with an air humidity of 90% and a temperature of 25 °C for 48 h. After 48 h of humidity conditioning, switch the Material Moisture Gigamodule to the "Ohmic resistance [10 × Log(R)]" mode, connect it with the probe using alligator clips, and collect its resistance value and weight. Subsequently, the relative humidity of the air was increased by 5%, when the specimens weight change was less than 0.01 g, the weight and the resistance value were measured, and this step was repeated until the relative humidity of the air was adjusted to 90%.

The moisture content obtained by the weighing method is calculated according to Eq. (15).

$$M = \frac{m - m_0 - m_n}{m_0} \qquad (15)$$

where, $M$ represents the moisture content; $m_0$ represents the dry weight of wood; $m_n$ represents the probe weight.

The calibration file is automatically generated by the software Soft-FOX 3.00 in a table containing the "resistance value" and the gravimetrically determined "wood moisture content value".

### 3.2. Experiment configuration

The moisture content of the wood was collected by a data logger (Thermofox Universal) and a universal sensor extension module (Material Moisture Gigamodule) (Figure 4(a)). Software SoftFOX 3.00 (Scanntronik Mugrauer GmbH) was used to calculate moisture content from resistance recordings. The software provides pre-programmed conversion formulas for untreated wood [36].

The center of the middle layer board was measured at Locations A1 and A2, the center of the outer layer board at Locations B1 and B2 measure, the middle layer board at 22.5 mm from the central at Locations

C1 and C2, the middle layer board at 22.5 mm from the central at Locations D1 and D2 and Locations E2 and F2 are measured at the edges, as shown in Figure 5(a). And the texture direction of the three layers is shown in Figure 5(b).

### 3.3. Experiments with different texture

To verify the validity of the method, we conducted two types of experiments: constrained boundary and free boundary. The constrained boundary is to verify the validity of the inner boundary conditions, and the proposed model with inner boundary conditions is not disturbed by the texture in the case of single-direction diffusion. The free boundary is to demonstrate that the fiber orientation is considered in this model. Due to the limitation of the number of measuring points of the moisture content detector, the test is carried out in two times: the test of parallel texture and the test of vertical texture.

#### 3.3.1. The test of parallel texture

Each group of No. 1–3 specimen was placed in a climate chamber with an air humidity of 90% and a temperature of 25 °C for adjustment. After 9 days, the four sides (90 mm × 15 mm) of the specimens in group B were coated with silica gel for insulation treatment, and then put back in
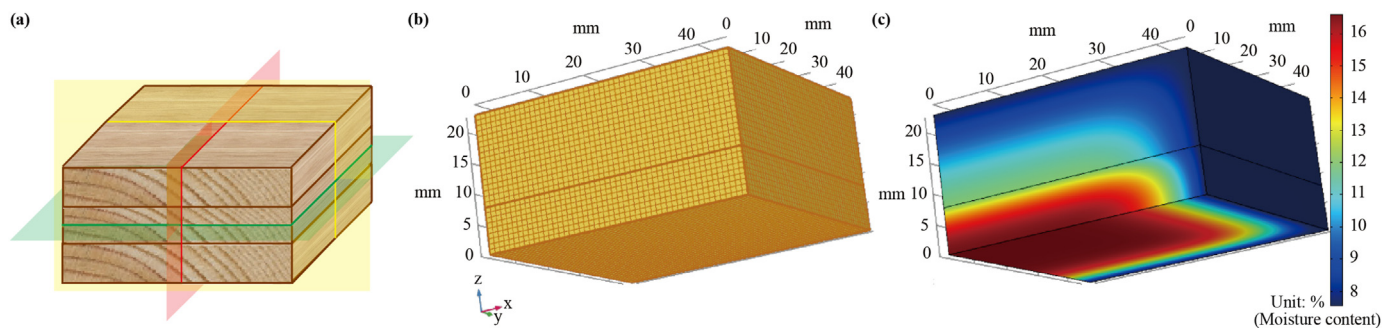


**Figure 7.** (a) Schematic diagram of the neutral layer; (b) Schematic diagram of finite element; (c) The result of the simulation.

**Table 3.** The coefficient of simulation test.

| | Location | The texture of flux surface | | | | | | The initial MC (%) | |
|---|---|---|---|---|---|---|---|---|---|
| | | The moisture diffusion coefficient (m$^2$/s) | | | The surface emission coefficient (m/s) | | | Parallel texture | Vertical texture |
| | | RT | LR | LT | RT | LR | LT | | |
| Location A1 | Outer | 1.6e − 10 | 1.4e − 10 | 5.4e − 10 | 1.3e − 5 | 5.9e6 | 3.24e − 6 | 24.0 | 12.0 |
| | Middle | 1.6e − 10 | 1.4e − 10 | 7.0e − 11 | | | 1.86e − 7 | 24.8 | 12.8 |
| Location B1 | Outer | 2.1e − 10 | 1.8e − 10 | 7.0e − 10 | 1.3e − 5 | 5.9e6 | 3.24e − 6 | 15.0 | 20.1 |
| | Middle | 2.1e − 10 | 1.8e − 10 | 9.1e − 11 | | | 1.86e − 7 | 15.0 | 20.0 |
| Location C1 | Outer | 2.1e − 10 | 1.8e − 10 | 7.0e − 10 | 1.3e − 5 | 5.9e6 | 3.24e − 6 | 15.0 | 20.0 |
| | Middle | 2.1e − 10 | 1.8e − 10 | 9.1e − 11 | | | 1.86e − 7 | 12.9 | 15.0 |
| Location D1 | Outer | 1.3e − 10 | 1.1e − 10 | 4.3e − 10 | 1.3e − 5 | 5.9e6 | 3.24e − 6 | 20.1 | 17.8 |
| | Middle | 1.3e − 10 | 1.1e − 10 | 5.6e − 11 | | | 1.86e − 7 | 20.0 | 18.0 |
| Location A2 | Outer | 3.2e − 10 | 2.5e − 10 | 1.58e − 9 | 1.3e − 5 | 5.9e6 | 3.24e − 6 | 15.6 | 19.0 |
| | Middle | 3.2e − 10 | 2.5e − 10 | 1.7e − 10 | | | 1.86e − 7 | 20.2 | 19.0 |
| Location B2 | Outer | 3.2e − 10 | 2.5e − 10 | 1.58e − 9 | 1.3e − 5 | 5.9e6 | 3.24e − 6 | 22.3 | 21.4 |
| | Middle | 3.2e − 10 | 2.5e − 10 | 1.7e − 10 | | | 1.86e − 7 | 23.1 | 21.4 |
| Location C2 | Outer | 1.6e − 10 | 1.4e − 10 | 1.58e − 9 | 1.3e − 5 | 5.9e6 | 3.24e − 6 | 15.5 | 15.0 |
| | Middle | 1.6e − 10 | 1.4e − 10 | 1.7e − 10 | | | 1.86e − 7 | 17.8 | 20.2 |
| Location D2 | Outer | 3.2e − 10 | 2.5e − 10 | 1.58e − 9 | 1.3e − 5 | 5.9e6 | 3.24e − 6 | 16.4 | 18.0 |
| | Middle | 3.2e − 10 | 2.5e − 10 | 1.7e − 10 | | | 1.86e − 7 | 21.7 | 21.0 |
| Location E2 | Outer | 3.2e − 10 | 2.5e − 10 | 1.58e − 9 | 1.3e − 5 | 5.9e6 | 3.24e − 6 | 16.6 | 12.0 |
| | Middle | 3.2e − 10 | 2.5e − 10 | 1.7e − 10 | | | 1.86e − 7 | 17.4 | 19.4 |
| Location F2 | Outer | 2.1e − 10 | 1.8e − 10 | 7.0e − 10 | 1.3e − 5 | 5.9e6 | 3.24e − 6 | 14.4 | 14.8 |
| | Middle | 2.1e − 10 | 1.8e − 10 | 9.2e − 11 | | | 1.86e − 7 | 26.4 | 24.2 |

the climate chamber to wait for the silica gel to dry and continue to adjustment. In order to reduce the impact of installing probes, only one set of probes was installed on each three-layer board. After a total of 13 days of conditioning, the specimens A-No. 3, C-No. 2, G-No. 3 and I-No. 2 were punched holes and inserted probe as shown in Figure 6(a), the

specimens B-No. 3, D-No. 2, H-No. 3 and J-No. 2 were punched holes and inserted probe as shown in Figure 6(b), the specimen F-No. 2 was punched holes as shown in Figure 6(c), and inserted probe as the outer layer board as Figure 6(d), and the specimens E-No. 2 was insert the probe with 7.5 mm as shown in Figure 6(e). The diameter of the hole is 3
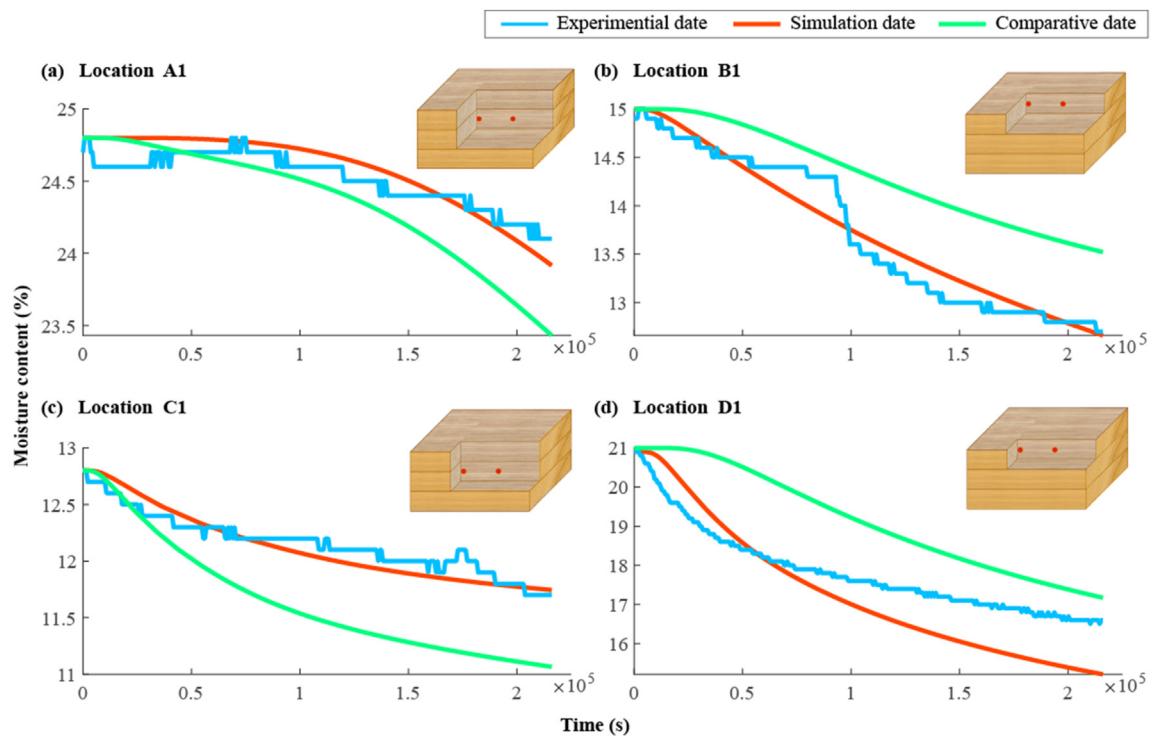


**Figure 8.** The experimental results for the parallel texture with constrained boundary condition (a) at location A1; (b) at location B1; (c) at location C1; (d) at location D1.
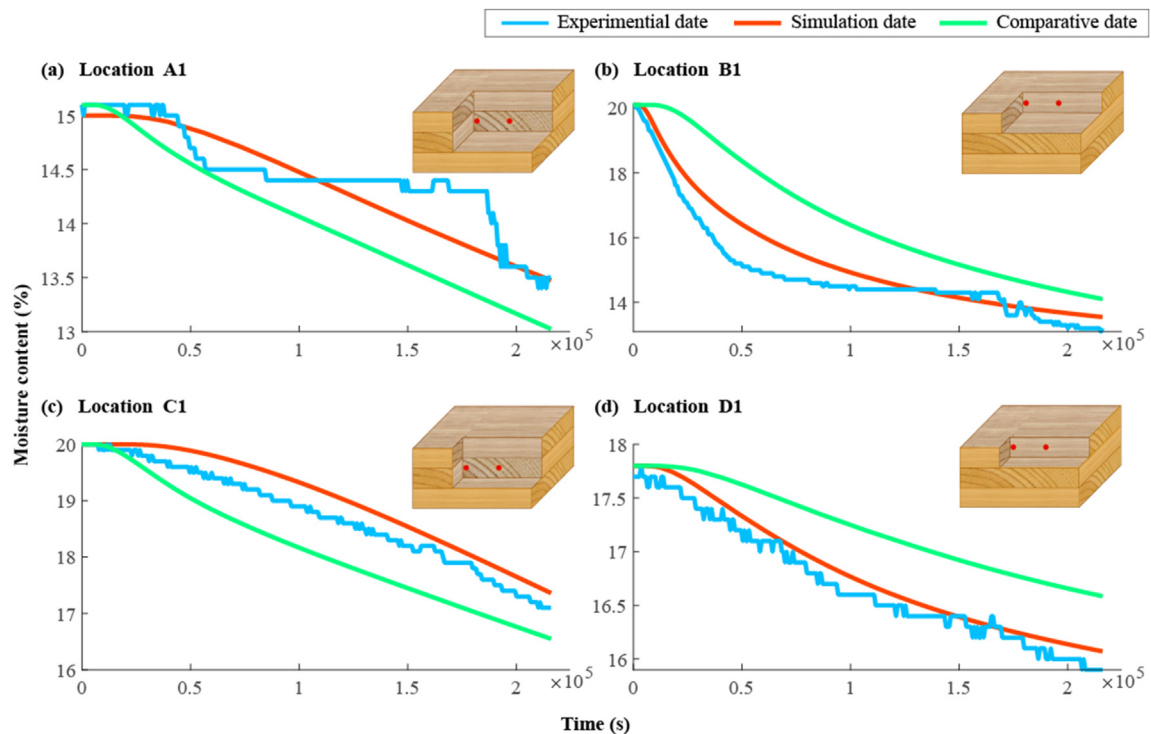


**Figure 9.** The experimental results for the vertical texture with constrained boundary condition (a) at location A1; (b) at location B1; (c) at location C1; (d) at location D1.

mm, the diameter of the probe is 2 mm, and the gap between the probe and the hole is sealed with insulating glue. Then put it back in the climate chamber for adjustment for a day.

After the adjustment is completed, the specimens A-No. 3, B-No. 3, F-No. 3, G-No. 3, H-No. 3 was placed in the middle layer as shown in Figure 4(b), the specimens C-No. 2, D-No. 2, E-No. 2, F-No. 2, I-No. 2, J-No. 2 were placed on the first layer as shown in Figure 4(b), and then all No. 1 specimens of A-J groups were placed on the third layer as shown in Figure 4(b), the other samples were filled with three layers, and the grain direction is shown in Figure 4(b). The fixing three-layer specimen was placed on the wooden track (Figure 4(a)), then connect the moisture content detector and the probe with alligator clips, and adjust the climate chamber to adjust the air humidity to 40% and the temperature to 25 °C for a 3 days experiment. And the initial moisture content of each layer board is as shown in Table 1.

### 3.3.2. The test of vertical texture

All the test specimens were disconnected from the moisture content detector, then still placed then the climate chamber with an air humidity of 90% and a temperature of 25 °C for adjustment and replace the F-No. 4 with F-No. specimen as the middle layer. After 10 days of conditioning, it

was fixed according to the first text. The difference from the first experiment was that the middle layer boards were all rotated 90°, as shown in Figure 4(c), the surface texture of the middle board was perpendicular to the first and third boards. The fixing the three-layer specimens was then placed on the wooden track, and alligator clips were as the connect equipment between the moisture content detector and the probes. Finally adjust the climate chamber with air humidity 40% and the temperature 25 °C for a 3 day experiment. And the initial moisture content of each layer board is as shown in Table 2.

### 3.4. Finite element model test of three-layer board

As shown in Figure 7(a), the three-layer board can be divided into eight sections. As the moisture diffuses outwards from the neutral layer before the equilibrium moisture content is reached. And the neutral layer in each of the three directions is the red, yellow and green faces in Figure 7(a). Ideally the diffusion is the same for all eight parts, so the mathematical model was established as 1/8 of the neutral layer outwards. And the finite element model with the same initial conditions and boundary conditions as the above mathematical model was also established in Figure 7(b) and 7(c) shows a result of parallel texture with free
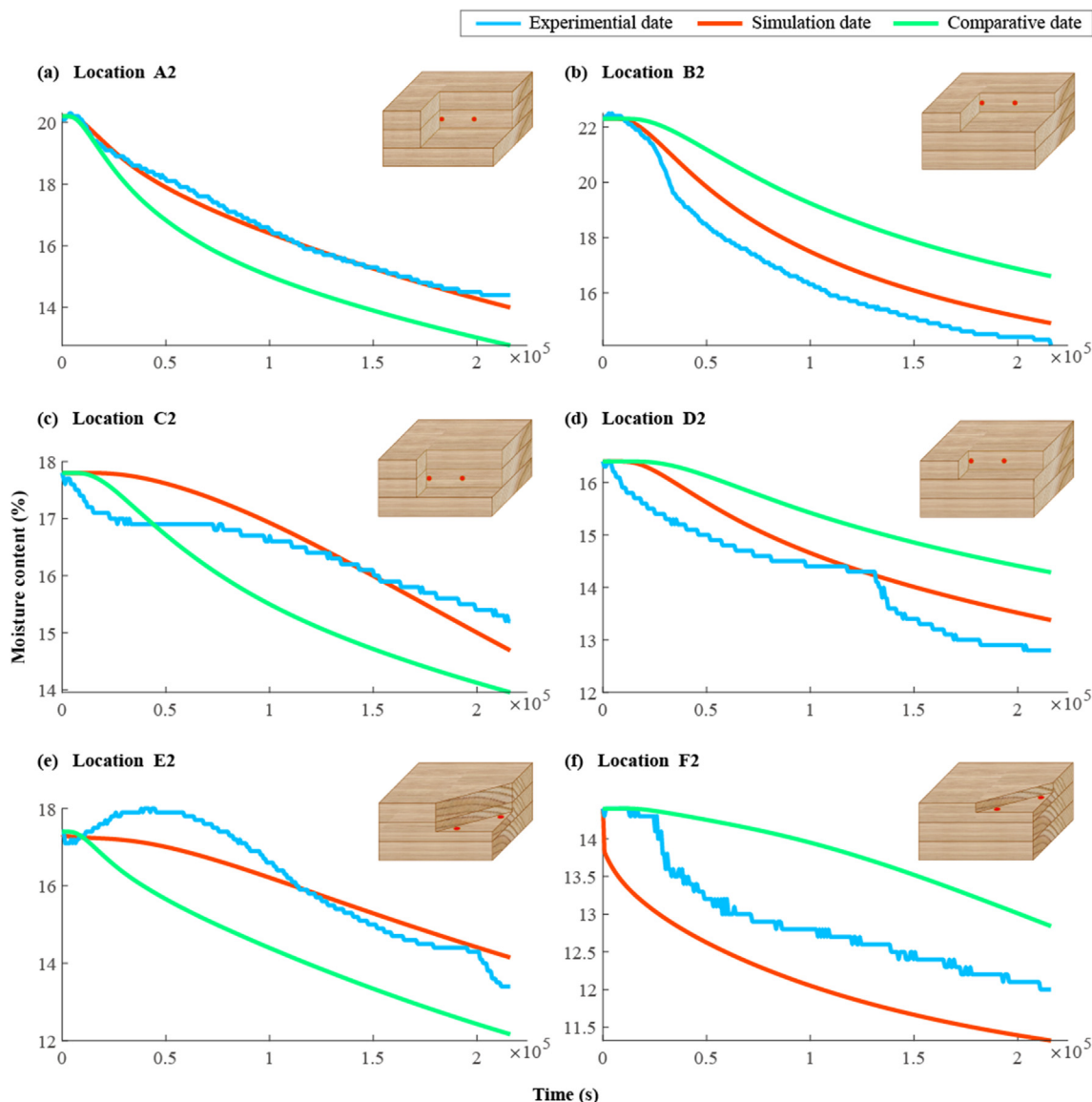


**Figure 10.** The experimental results for the parallel texture with free boundary condition (a) at location A2; (b) at location B2; (c) at location C2; (d) at location D2; (e) at location E2; (f) at location F2.

boundary condition. Different from the proposed boundary model, the interface between the middle layer board and outer layer board only exists in a geometric with no practical significance in physical changes. Hence, the above model is hereinafter named as simple boundary model. The diffusion videos of the two moisture diffusion boundary models with four types (constrained boundary with parallel texture, constrained boundary with vertical texture, free boundary with parallel texture, free boundary with vertical texture) are as shown in the **Supplementary Material** where the initial moisture content of the middle board is 17.8% and the initial moisture content of the outer board is 15.5%. In the proposed boundary model, air relative humidity is used as a necessary input, and the moisture content corresponding to air relative humidity is calculated using a modified version of the equation suggested by Glass et al. [37], and the modified result of Lie et al. is used as the conversion formula in this manuscript [36].

$$M_{RH} = (-\frac{In(1-RH)}{26.665})^{1/1.523} \qquad (16)$$

where, $M_{RH}$ represents the wood moisture content corresponding to the air relative humidity, which indicates the equilibrium moisture content of the wood board at 25 °C; $RH$ represents the air relative humidity.

The other coefficient in the proposed boundary model were determined according to the Dincer's method. Except the surface emission coefficient of the middle layer board was not set specifically, the coefficients of the simple boundary model are exactly the same as those of the proposed boundary model. The parameters measured by the simulation are shown in Table 3, in which the moisture diffusion coefficient and surface emission coefficient were carried out by the method of Section 3.1.1.

## 4. Results and discussion

### 4.1. Experimental and simulation result

The experimental results show the moisture content at different monitoring points under different boundary conditions. Figures 8 and 9 show the actual and simulated changes of moisture content at the four measuring points of the three-layer board with constrained boundary. As
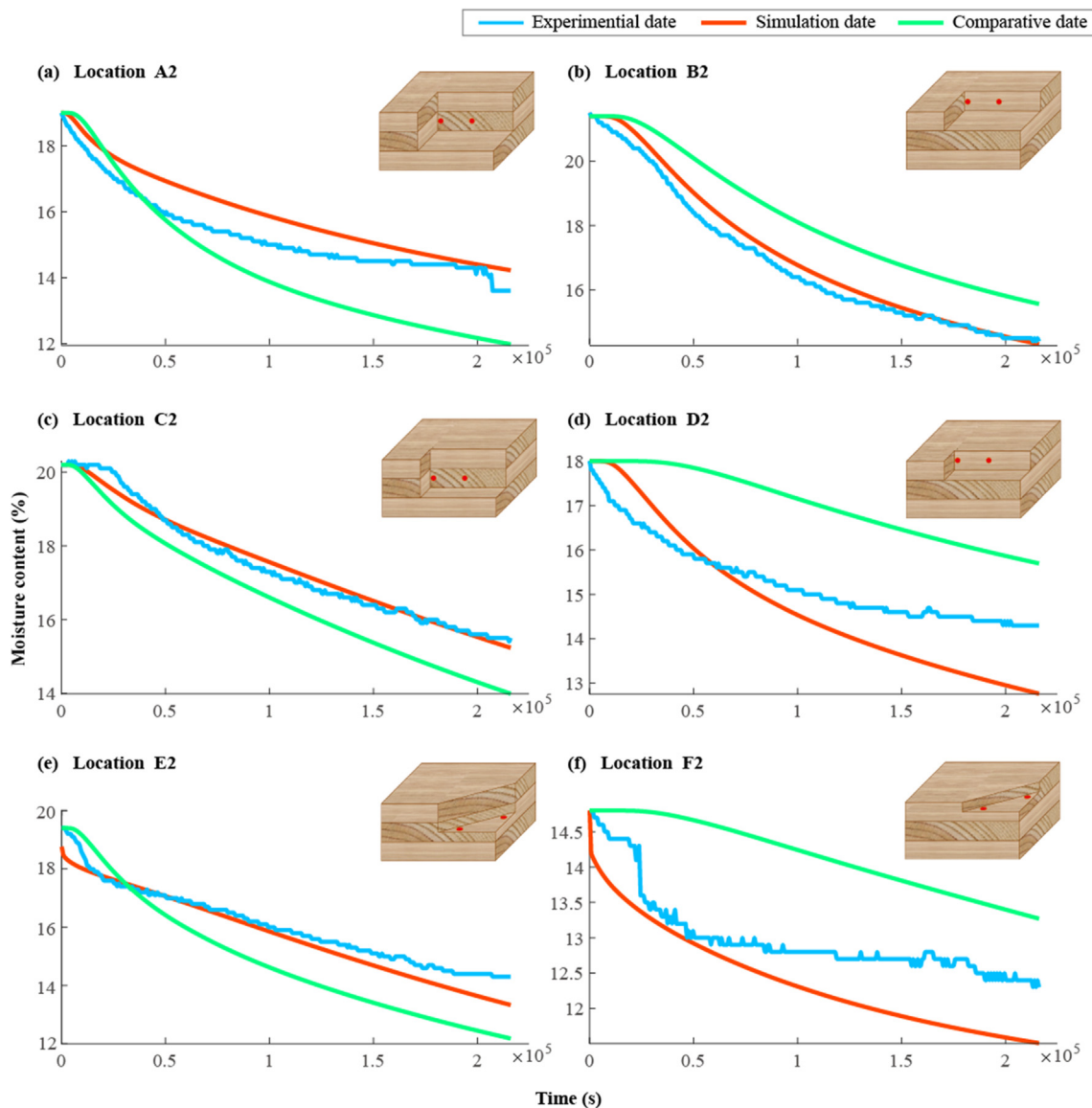


**Figure 11.** The experimental results for the vertical texture with free boundary condition (a) at location A2; (b) at location B2; (c) at location C2; (d) at location D2; (e) at location E2; (f) at location F2.

shown in the figures, the simulation date was extracted by the proposed boundary model, and the comparative date extracted by the simple boundary model. The texture directions of the boards are as shown in Figure 3(b) and 3(c), respectively. Figures 8(a) and 9(a) represent the change in moisture content at the center of the middle board, Figures 8(b) and 9(b) represent the change in moisture content at the center of the outer layer board, Figures 8(c) and 9(c) represent the change of moisture content from the center of the middle board to the half of the boundary, and Figures 8(d) and 9(d) represent the change of moisture content from the center of the middle board to the half of the boundary.

In Figures 8(b) and 9(a), the actual measurement curves are abnormal, but the overall trend of the actual curves and the simulated result curves are consistent, which may be caused by the poor contact of the probe. Consistent with the conjecture, due to the simple boundary model reflects the total change, the difference between the actual experiment and simple boundary model is larger than the difference between the proposed boundary model. And as shown in Figures 8 and 9, the comparison results between the simple boundary model and the actual experiment is consistent. As shown in Table 3, regardless of the moisture diffusion coefficient or the surface emission coefficient, the coefficient of the middle layer board was smaller than that of the outer layer board with the flux surface of LR. Hence, the diffusion speed of the middle layer board is slower than that of the outer layer board in the actual diffusion, which was not take into account in the simple boundary model. Therefore, the moisture content of the middle layer board measurement points is lower than the actual, and the outer layer board is higher than the actual.

Figures 10 and 11 show the actual and simulated changes of moisture content at the six locations of the board with free boundary conditions. The texture direction of three-layer board is as shown in Figure 3(b) and 3(c), respectively. Figures 10(a) and 11(a) represent the change in moisture content at the center of the middle board, Figures 10(b) and 11(b) represent the change in moisture content at the center of the outer layer board, Figures 10(c) and 11(c) represent the change of moisture content from the center of the middle board to the half of the boundary, Figures 10(d) and 11(d) represent the change of moisture content from the center of the middle board to the half of the boundary, and Figures 10(e) and 11(e) represent the middle board changes in moisture content near a corner (Figure 6(e)), Figures 10(f) and 11(f) show the change of moisture content near a corner of the middle board (Figure 6(d)).

The variation of the actual measured moisture content at Figure 10(c) is quite different from the simulated one, because the moisture diffusion coefficient and the surface emission coefficient coefficients selected for the simulation are smaller than those of the actual wood. Resulting in an upwardly convex form of the simulated curve, while the actual measured curve is approximately a downward concave curve. Figure 10(e) shows an increase at first and then a decrease in the actual measurement. This is because one of the outer layer board has a moisture content of 24.8%, and the moisture content of the outer board is higher than that of the middle board, so that the moisture content first increases and then decreases. But the moisture content of the outer board was selected in the simulation is only 16.6%, which is similar to the middle board (17.4%), so the simulation curve is stable. Figure 11(f) show the same trend at the beginning of the actual measurement, which may be caused by the same probes and the same sensor. As shown in Figures 10 and 11, the changed boundary conditions did not affect the accuracy of the simple boundary model and the proposed boundary model. And the difference between the actual experiment and the simple boundary model is still larger than the difference between the proposed boundary model. The same as the constrained boundary, the moisture content of the middle layer board measurement points is lower than the actual, and the outer layer board is higher than the actual.
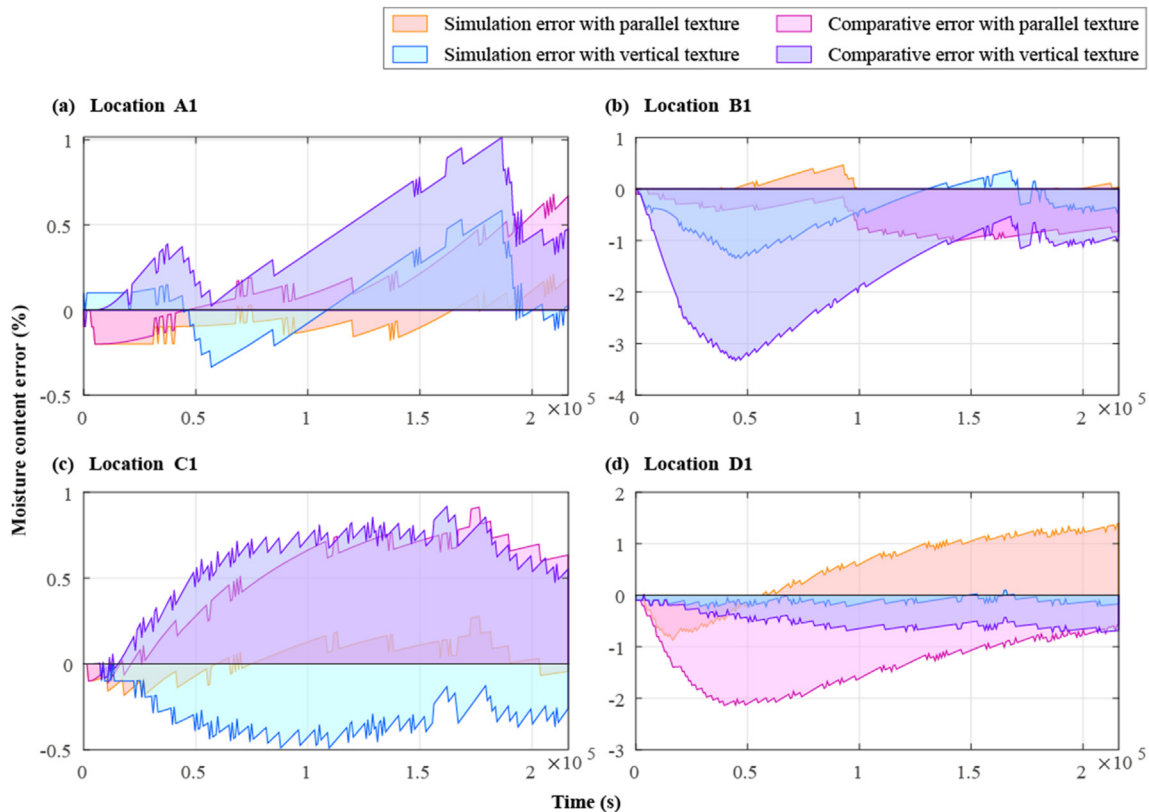


**Figure 12.** Moisture content error with constrained boundary condition (a) at location A1; (b) at location B1; (c) at location C1; (d) at location D1.

## 4.2. Error analysis between experimental and simulation

The errors of the parallel texture test and its corresponding two simulations in free diffusion, and the errors of the vertical texture test and its corresponding two simulations are both shown in Figure 12. Figure 12(a) represents the four types of errors at the center of the middle layer board, Figure 12(b) represents the four types of errors at the center of the outer layer board, Figure 12(c) represent the four types of errors from the center of the middle layer board to the half of the boundary, and Figure 12(d) represent the four types of errors from the center of the middle layer board to the half of the boundary.

The errors of the parallel texture test and its corresponding two simulations in the constrained diffusion, and the errors of the vertical texture test and its corresponding two simulations are both shown in Figure 13. Figure 13(a) represents the four types of errors at the center of the middle layer board, Figure 13(b) represents the four types of errors at the center of the outer layer board, Figure 13(c) represents the four types of errors from the center of the middle layer board to the half of the boundary, Figure 13(d) a represents the four types of errors from the center of the middle layer board to the half of the boundary, and Figure 13(e) represents the four types of errors near a corner

(Figure 6(e)), Figure 13(f) represents the four types of errors near a corner of the middle layer board (Figure 6(d)).

All errors with the proposed boundary model are less than 2% (moisture content), and 3.4% (Eq. (16)) in the simple boundary model in Figures 12 and 13. And the error with simple boundary model is larger than the proposed boundary model in every point, which indicates the accuracy of the proposed boundary model.

$$e = M_t - M_s \tag{17}$$

where, $e$ represents the moisture content error between the test moisture content and the simulation moisture content, $M_t$ represents the test moisture content and $M_s$ represents the test moisture content.

The apparent regularity is shown by the error bar of the simple boundary model in Figure 14. As described above, the simple boundary conditions do not take into account the difference of the moisture diffusion coefficient and surface emission coefficient between the middle and outer layer board, so the error of the middle layer board is greater than 0, and the error of the outer layer board is less than 0. Due to the boundary were considered, the proposed boundary model didn't exhibit obvious regularity.
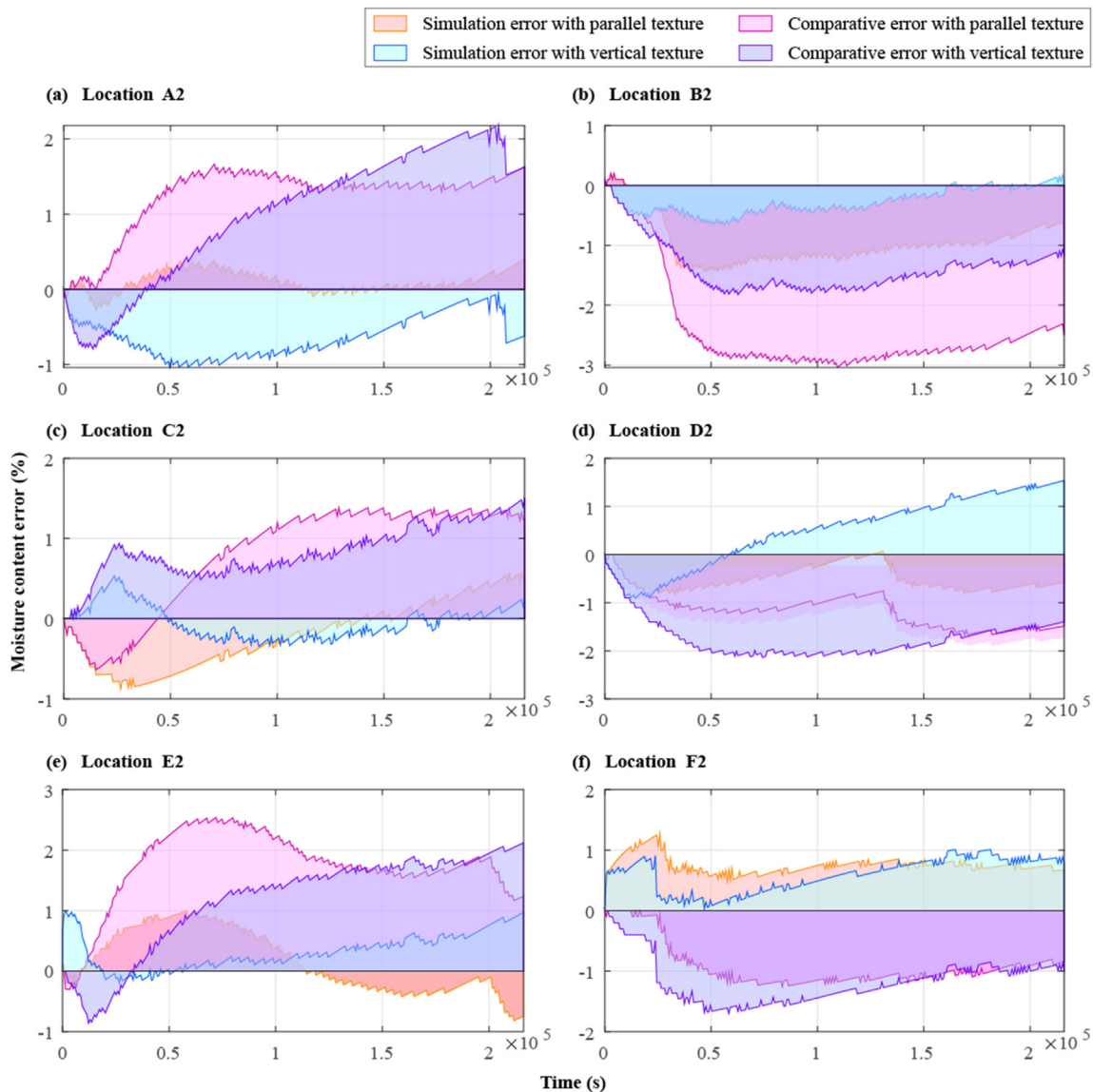


**Figure 13.** Moisture content error with free boundary condition (a) at location A2; (b) at location B2; (c) at location C2; (d) at location D2; (e) at location E2; (f) at location F2.
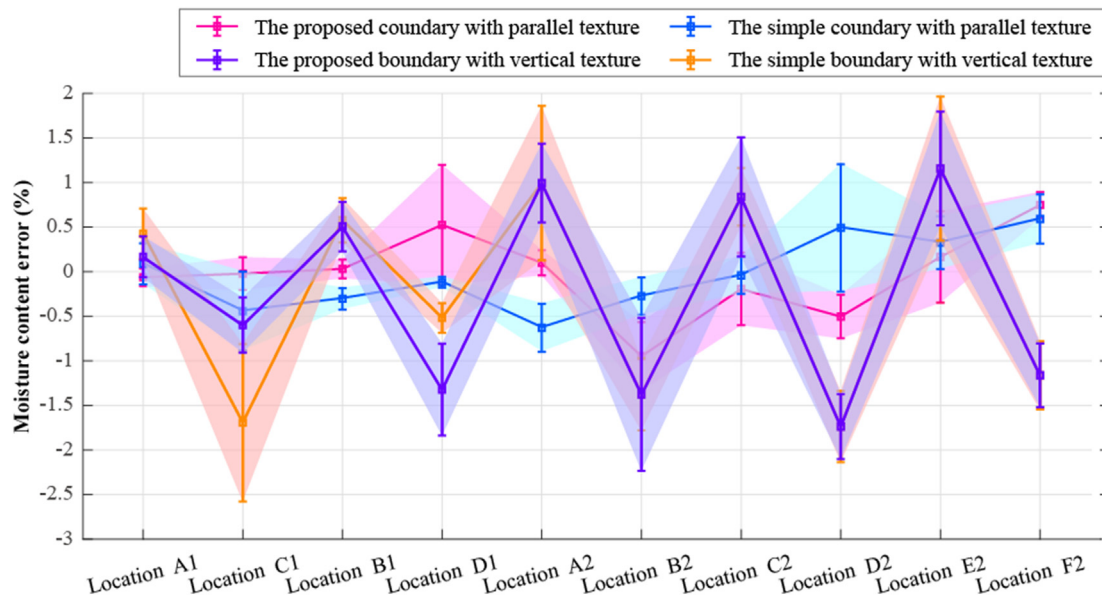
**Figure 14.** The error bar of different boundary conditions with two models.
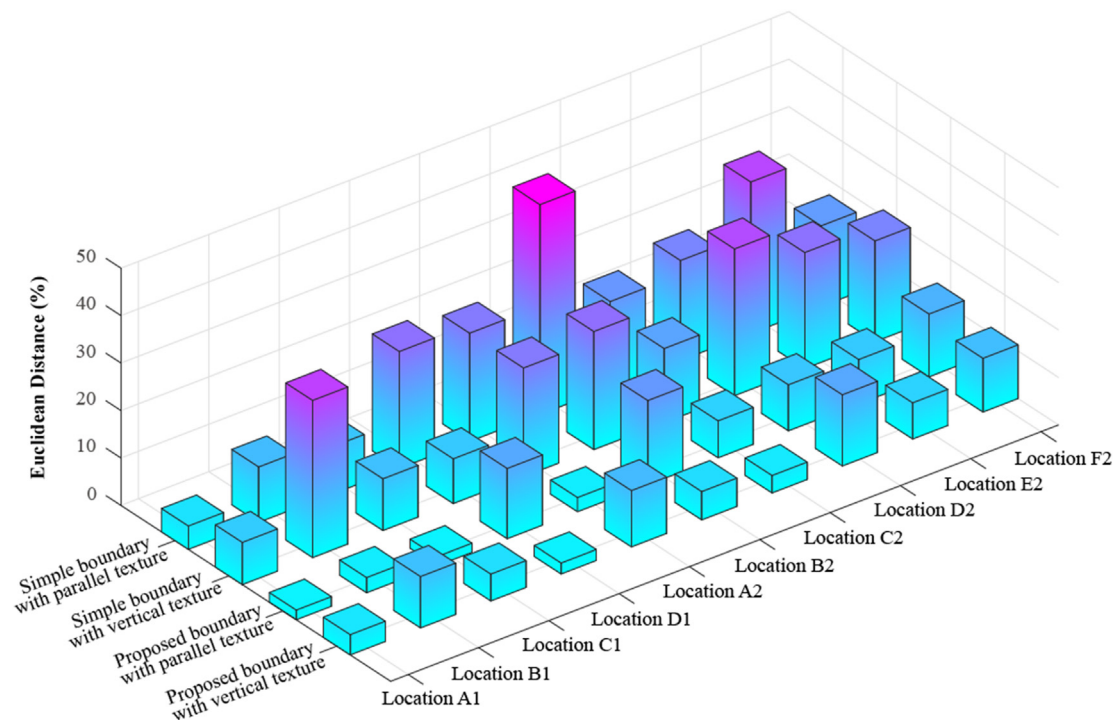


**Figure 15.** Correlation of actual and experimental values.

Figure 15 represents the Euclidean distance of simulation and experimental with different boundary conditions, respectively. On the whole, the Euclidean distance of the proposed boundary condition simulation data with the actual experiment data is smaller than that of the simple boundary condition simulation data, which shows that the simulation data of the proposed boundary condition are more in line with the actual experimental data. From the perspective of fiber orientation, the Euclidean distance of the proposed boundary condition simulation data with the actual experiment data is smaller than the simulation data of the simple boundary condition, whether it is a parallel texture or a vertical texture, which indicates that the fiber orientation does not have a great impact on the model.

## 5. Conclusion

The mathematical model for three-layer board with complex boundary conditions that establish by this manuscript was ability to predict moisture content within wood in complex situations. The validity of the inner boundary conditions was verified by tests with constrained boundary conditions, and the role of fiber orientation was demonstrated by tests with free diffusion. The experimental and simulation results show that the proposed boundary condition committed to build a high-accuracy moisture diffusion model. Different from the simple boundary model, the proposed boundary model considers more comprehensively, which results in high accuracy of moisture content in both middle and

outer layer board. This present model is not only suitable for the moisture content analysis of wood but also for other sparse porous materials.

However, the accuracy of the moisture diffusion coefficient and surface emission coefficient, which has influenced by temperature and moisture content, has a decisive impact on the model. To overcome its limitations, experimental study can be carried out to determine the relationship between temperature and moisture content and improve the model accuracy.

## Declarations

### Author contribution statement

Xueyi Ma: Conceived and designed the experiments; Performed the experiments; Analyzed and interpreted the data; Wrote the paper.

Dong Zhao: Conceived and designed the experiments; Contributed reagents, materials, analysis tools or data.

Chenyu Yao: Performed the experiments.

Jian Zhao: Conceived and designed the experiments; Contributed reagents, materials, analysis tools or data; Wrote the paper.

### Funding statement

### Data availability statement

Data will be made available on request.

### Declaration of interests statement

The authors declare no conflict of interest.

### Additional information

Supplementary content related to this article has been published online at https://doi.org/10.1016/j.heliyon.2022.e10626.

## References

[1] A. Pan, W. Zhang, Q. Xie, L. Dai, Y. Zhang, Do carbon emissions accelerate low-carbon innovation? Evidence from 285 Chinese prefecture-level cities, Environ. Sci. Pollut. Control Ser. 28 (2021) 50510–50524.

[2] A. Dodoo, Life cycle primary energy use and carbon emission of residential buildings, Mittuniversitetet (2011).

[3] J. Malinen, M. Pesonen, T. Määttä, M. Kajanus, Potential harvest for wood fuels (energy wood) from logging residues and first thinnings in Southern Finland, Biom. Bioener. 20 (3) (2011) 189–196.

[4] Y. Sun, K. Panchabikesan, F. Haghighat, J.T. Luo, M. Robichaud, Development of advanced controllers to extend the peak shifting possibilities in the residential buildings, J. Build. Eng. 43 (2) (2021), 103026.

[5] S.J. Pang, J.K. Oh, C.Y. Park, S.J. Kim, J.J. Lee, Effects of Size Ratios on Dovetail Joints in Korean Traditional Wooden Building, Toyowa Journal of the Humanities & Social Sciences, 2012.

[6] Q. Zhao, D. Zhao, J. Zhao, L. Fei, The song dynasty shipwreck monitoring and analysis using acoustic emission technique, Forests 10 (9) (2019) 767.

[7] SETRA, Les ponts en bois: comment assurer leur durabilité (Timber bridges: how to ensure their durability), in: SETRA (Service d'Etudes Technique des Routes et Auto-routes), 2006. France.

[8] C.A. Chávez, N.O. Moraga, C.H. Salinas, R.C. Cabrales, R.A. Ananías, Modeling unsteady heat and mass transfer with prediction of mechanical stresses in wood drying, Int. Commun. Heat Mass Tran. 123 (2021), 105230.

[9] V. Angst, K.A. Malo, The effect of climate variations on glulam—an experimental study, European J. Wood & Wood Prod. 70 (2012) 603–613.

[10] S. Svensson, T. Toratti, Mechanical response of wood perpendicular to grain when subjected to changes of humidity, Wood Sci. Technol. 36 (2002) 145–156.

[11] S. Vesper, C. Mckinstry, D. Cox, G. Dewalt, Correlation between ERMI values and other moisture and mold assessments of homes in the American healthy homes survey, J. Urban Health 86 (6) (2009) 850–860.

[12] N. Björngrim, P.A. Fjellström, O. Hagman, Resistance measurements to find high moisture content inclusions adapted for large timber bridge cross-sections, Bioresources 12 (2017) 3570–3582.

[13] E.F. Hansson, C. Brischke, L. Meyer, T. Isaksson, S. Thelandersson, D. Kavurmaci, Durability of timber outdoor structures - modelling performance and climate impacts, in: Proceedings of 12th World Conference on Timber Engineering, 2012. Auckland.

[14] N. Mendes, I. Ridley, R. Lamberts, P.C. Philippi, K. Budag, UMIDUS: a PC program for the prediction of heat and moisture transfer in porous building elements, Build. Simulat. Conf.-IBPSA 99 (1999) 277–283.

[15] Z. Pasztory, P.N. Peralta, S. Molnar, I. Peszlen, Modeling the hygrothermal performance of selected North American and comparable European wood-frame house walls, Energy Build. 49 (2012) 142–147.

[16] Y.A. Gatica, C.H. Salinas, R.A. Ananias, Modeling conventional one-dimensional drying of radiata pine based on the effective diffusion coefficient, Lat. Am. Appl. Res. 41 (2011) 183–189.

[17] E. Vereecken, S. Roels, Wooden beam ends in combination with interior insulation: an experimental study on the impact of convective moisture transport, Build. Environ. 148 (2019) 524–534.

[18] X. Zhou, J. Garmeliet, D. Derome, Assessment of moisture risk of wooden beam embedded in internally insulated masonry walls with 2D and 3D models, Build. Environ. 193 (2021), 107460.

[19] N. Mendes, F.C. Winkelmann, R. Lamberts, P.C. Philippi, Moisture effects on conduction loads, Energy Build 35 (7) (2003) 631–644.

[20] J. Berger, S. Guernouti, M. Woloszyn, C. Buhe, Factors governing the development of moisture disorders for integration into building performance simulation, J. Build. Environ 3 (2015) 1–15.

[21] N.S. Bunkholt, P. Rüther, L. Gullbrekken, S. Geving, Effect of forced convection on the hygrothermal performance of a wood frame wall with wood fibre insulation, Build. Environ. 195 (2021), 107748.

[22] S. Avramidis, J.F. Siau, An investigation of the external and internal resistance to moisture diffusion in wood, Wood Sci. Technol. 21 (3) (1987) 249–256.

[23] C. Skaar, Wood-water relations, QRB (Q. Rev. Biol.) (1988).

[24] L. Wadso, Measurements of water vapor sorption in wood: Part 2. Results, Wood Sci. Technol 28 (1993) 59–65.

[25] S.Q. Shi, Diffusion model based on Fick's second law for the moisture adsorption process in woodfiber-based composites: is it suitable or not, Wood Sci. Technol. 41 (2007) 645–658.

[26] M. Rauma, G. Johanson, Assessment of dermal absorption by thermogravimetric analysis: development of a diffusion model based on Fick's second law, J. Pharmaceut. Sci. 98 (11) (2009) 4365–4375.

[27] Daniel Konopka, Michael Kaliske, Transient multi-Fickian hygro-mechanical analysis of wood, Comput. Struct. 197 (1) (2018) 12–27.

[28] S. Florisson, J. Vessby, W. Mmari, S. Ormarsson, Three-dimensional orthotropic nonlinear transient moisture simulation for wood: analysis on the effect of scanning curves and nonlinearity, Wood Sci. Technol. 54 (2020) 1197–1222.

[29] S. Florisson, J. Vessby, S. Ormarsson, A three-dimensional numerical analysis of moisture flow in wood and of the wood's hygro-mechanical and visco-elastic behaviour, Wood Sci. Technol. 55 (2022) 1–36.

[30] Y. Wen, P. Yang, J. Zhao, D. Zhao, Determination of effective coefficient of Chinese fir (cunninghamia lanceolata) during adsorption and desorption process, Wood Fiber Sci. 51 (2019) 364–374.

[31] Ibrahim Dincer, Moisture loss from wood products during drying – part I: moisture diffusivities and moisture transfer coefficients, Energy Sources 20 (1) (1998) 67–75.

[32] J. Zhao, W. Dai, T. Niu, Fourth-order compact schemes of a heat conduction problem with Neumann boundary conditions, Numer. Methods Part. Differ. Equ. 23 (5) (2007) 949–959.

[33] S. Ozawa, S. Roppongi, Singular variation of domain and eigenvalues of the Laplacian with the third boundary condition, Proc. Jpn. Acad. 68 (7) (1992) 186–789.

[34] Service U., Stresses in Laminated wood Construction, U.S. Dept. of Agriculture, Forest Service, Forest Products Laboratory, 1952.

[35] J. Zhan, J. Gu, Y. Cai, Analysis of moisture diffusivity of larch timber during convective drying condition by using Crank's method and Dincer's method, J. For. Res. 18 (3) (2007) 199–203.

[36] S.K. Lie, T.K. Thiis, G.I. Vestøl, O. Høibø, L.R. Gobakken, Can existing mould growth models be used to predict mould growth on wooden claddings exposed to transient wetting? Build. Environ. 152 (2019) 192–203.

[37] S.V. Glass, S.D. Gatland, K. Ueno, C.J. Schumacher, Analysis of improved criteria for mold growth in ASHRAE standard 160 by comparison with field observations, in: P. Mukhopadhyaya, D. Fisler (Eds.), Hygrothermal Performance of Building Envelopes: Materials, Systems and Simulations, ASTM STP1599, ASTM International, West Conshohocken, 2017.